One-dimensional Dexter-type excitonic topological phase transition

Jianhua Zhu [1,2,*] Haoxiang Chen,[1,†] Ji Chen,[1,3,4,‡] and Wei Wu [2,§]

[1]*School of Physics, Peking University, Chengfu Road 209, Haidian, Beijing 100871, China*
[2]*Department of Physics and Astronomy, University College London, Gower Street, London WC1E 6BT, United Kingdom*
[3]*Interdisciplinary Institute of Light-Element Quantum Materials and Research Center for Light-Element Advanced Materials,*
Peking University, Beijing 100871, People Republic of China
[4]*Frontiers Science Center for Nano-Optoelectronics, Peking University, Beijing 100871, People Republic of China*

The concept of the Su-Schrieffer-Heeger model, which was successfully introduced in topological photonics, can also be applied to the study of topological excitonics. Here we study the topological properties of a one-dimensional excitonic tight-binding model formed by two-level systems by taking into account the charge transfer and local excitations. The interactions between the two types of excitons give rise to a rich spectrum of physics, including the nontrivial topological phase in the uniform chain, unlike the conventional Su-Schrieffer-Heeger model, the topologically nontrivial flat bands, and, most importantly, the excitonic topological phase transition assisted by the Dexter electron exchange process. The excitonic topological phase leads to the development of "chiral superposition." The topological edge states are robust because they are protected by the inversion symmetry. Based on our calculations, experiments for observing the edge states optically in a molecular chain are proposed.

I. INTRODUCTION

The exciton, a bound state of an electron and a hole, is an important concept in optics and can be either delocalized (Wannier-Mott exciton) or localized (Frenkel exciton) [1]. The Frenkel exciton, normally formed in the insulator or the molecular crystal, migrates by two mechanisms, namely, Föster coupling and the Dexter electron exchange [2–8]. Föster coupling stems from the excitation energy transfer between physical entities. The Dexter electron exchange can be understood as the case in which the electrons on the upper and the lower levels hop in opposite directions simultaneously, resulting in the migration of the entire exciton [Fig. 1(a)]. The excitonic migration from the "antenna" pigment to the chemical reaction center responsible for energy transformation is of great importance for the photosynthetic process in plants [9–11]. The electron and hole can live either on the same site [local excitation (LE)] or on different ones [charge transfer (CT)]. Especially, the CT process is crucial for both life on Earth and our modern daily life relying on electricity [12]. Recent research suggested that the CT state could play an important role for improving the performance of organic light emitting diodes, solar cells, and resistive memory devices [13–15]. CT excited states can also mediate the transition in the Dexter electron exchange process [16].

Recent topical research on topological photonics (TP) attempted to construct the photonic topological state to control the flow of light, relying on a specially designed artificial structure [17–23]. On the other hand, the topological state could also arise from the natural topology of the interactions between particles. Studying topological states of this type is beneficial for deepening the understanding of fundamental optical phenomena in nature. One-dimensional (1D) chain structures, which can be formed by atoms, molecules, quantum dots, and semiconductor dopants, among others, recently attracted much attention due to their interesting topological properties [24–31]. The Su-Schrieffer-Heeger (SSH) model is a classic example of the topological phase transition in one dimension [Fig. 1(b)] [32,33]. The SSH model consists of two sublattices (L and R) linked by intracell and intercell couplings, whose competition determines the topological properties of the model. The chiral symmetry of the SSH model leads to an integer winding number ($\mathbb{Z}$ invariant). The corresponding Zak phase (the Berry phase for one dimension) can therefore take an integer number of π. The inversion symmetry further constrains the Zak phase to be either 0 (trivial) or π (nontrivial) under an additional mode of 2π [34,35], rendering a $\mathbb{Z}_2$ invariance. A topologically nontrivial phase with a Zak phase of π appears when the intercell hopping strength is greater than the intracell one. The SSH model has also been realized in TP [19]. A fascinating topic for TP in one dimension is the flat band, which recently stimulated intense research interest in condensed matter physics, photonics, and

---

*Contact author: ucapjhz@ucl.ac.uk
†Contact author: hxchen@pku.edu.cn
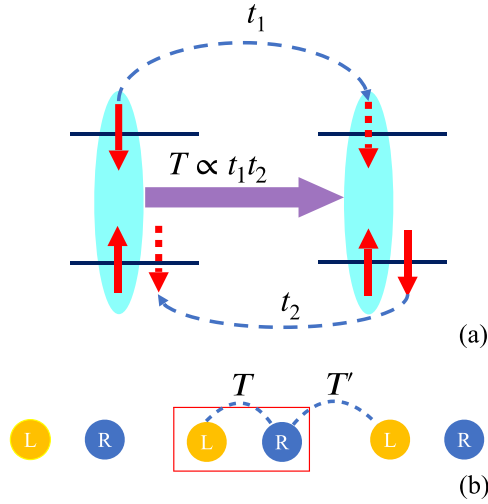‡Contact author: ji.chen@pku.edu.cn
§Contact author: wei.wu@ucl.ac.uk

FIG. 1. (a) The scheme for the Dexter electron exchange. $T(\propto t_1 t_2)$ is the effective hopping amplitude for the entire singlet exciton. (b) The SSH model consists of L and R sublattices, intracell hopping T, and intercell hopping T'.

metamaterials [36–42]. Moreover, the flat photonic band has many potential applications such as slow light due to the vanishing group velocity [36]. Similarly, the rich spectra of physics can be expected when introducing the idea of the SSH model to the excitonic systems.

Topological excitons have been discussed extensively for two-dimensional materials [43–47]. However, studies of the excitons in one dimension are still rare. Here we study the topological properties in the 1D excitonic model formed by the generic two-level systems coupled through the Dexter electron exchange, which takes into account the LE and CT excited states [48]. Both of these excited states are important for the optical and charge dynamics [49,50].

II. METHODS

Here we map out the six excitonic states, LE1 and 2 and CT1–CT4, in the unit cell to better illustrate the couplings between them, as shown in Fig. 2(a). The Hamiltonian reads

$$
\begin{aligned}
\hat{H} = \sum_n & \, t_2 a^\dagger_{\mathrm{LE1},n} a_{\mathrm{CT1},n} + t_1 a^\dagger_{\mathrm{LE1},n} a_{\mathrm{CT2},n} \\
& + t'_1 a^\dagger_{\mathrm{LE1},n} a_{\mathrm{CT3},n-1} + t'_2 a^\dagger_{\mathrm{LE1},n} a_{\mathrm{CT4},n-1} \\
& + t_1 a^\dagger_{\mathrm{LE2},n} a_{\mathrm{CT1},n} + t_2 a^\dagger_{\mathrm{LE2},n} a_{\mathrm{CT2},n} \\
& + t'_2 a^\dagger_{\mathrm{LE2},n} a_{\mathrm{CT3},n} + t'_1 a^\dagger_{\mathrm{LE2},n} a_{\mathrm{CT4},n} \\
& - \frac{d}{4} a^\dagger_{\mathrm{LE1},n} a_{\mathrm{LE1},n} - \frac{d}{4} a^\dagger_{\mathrm{LE2},n} a_{\mathrm{LE2},n} \\
& + \frac{d}{4} a^\dagger_{\mathrm{CT1},n} a_{\mathrm{CT1},n} + \frac{d}{4} a^\dagger_{\mathrm{CT2},n} a_{\mathrm{CT2},n} \\
& + \frac{d}{4} a^\dagger_{\mathrm{CT3},n} a_{\mathrm{CT3},n} + \frac{d}{4} a^\dagger_{\mathrm{CT4},n} a_{\mathrm{CT4},n} \\
& + \mathrm{H.c.} \tag{1}
\end{aligned}
$$

This Hamiltonian can be transformed into the momentum space as follows:

$$
\hat{H}_k = \begin{pmatrix}
-\frac{d}{2} & 0 & t_2 & t_1 & t'_1 e^{-ik} & t'_2 e^{-ik} \\
0 & -\frac{d}{2} & t_1 & t_2 & t'_2 & t'_1 \\
t_2 & t_1 & \frac{d}{2} & 0 & 0 & 0 \\
t_1 & t_2 & 0 & \frac{d}{2} & 0 & 0 \\
t'_1 e^{ik} & t'_2 & 0 & 0 & \frac{d}{2} & 0 \\
t'_2 e^{ik} & t'_1 & 0 & 0 & 0 & \frac{d}{2}
\end{pmatrix}. \tag{2}
$$

Due to the nature of the exciton, which has to connect two states, the unit cell of the model is chosen to be consistent with the following finite chain calculations, but this chosen unit cell is asymmetric, breaking the inversion symmetry in
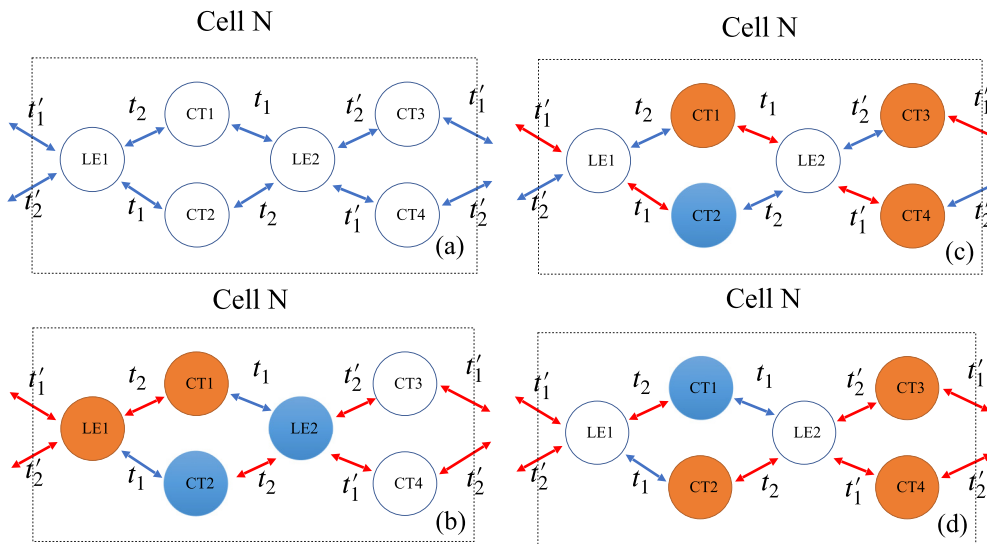

FIG. 2. (a) The model diagram in Ref. [48] mapped to a state-based structure with couplings and state labels. (b) An illustration of the two chiral superpositions (CSs) for $t_1 = 0$, $t_2 = 1$, and $t'_1 = t'_2 = x \neq 0$: the left-hand (L) state formed by LE1 and CT1 coupled by t_2 (in orange) and the right-hand (R) state formed by LE2 and CT2 (in blue). The LCS and RCS are decoupled by t_1. An illustration of the components in the eigenvectors for (c) $\{1, 0, 1, 0\}$ and (d) $\{0, 1, x, y\}$ with $|x^2 - y^2| = 1$. Here we use red (blue) to represent nonzero (zero) hopping. The L state is in orange, while the R state is in blue.

general. However, the infinite chain maintains the inversion symmetry. The couplings t_1 and t_2 are differentiated from t_1' and t_2' to account for dimerization. We set $d = 0$ in most of the paper because it does not affect the qualitative picture very much. We adopt the sequence $\{t_1, t_2, t_1', t_2'\}$ to describe our parameter set. Our calculation results not only are consistent with previous experimental and numerical works [51] but also, more importantly, can lead to a rich spectrum of physics, ranging from topologically nontrivial zero-mode flat bands to excitonic topological phase transitions.

We first solve the eigenvalues and eigenvectors for the Hamiltonian in the momentum space [Eq. (2)]. As the spectrum of the general case (nonzero in $\{t_1, t_2, t_1', t_2'\}$) shows the energies of the flat bands are always $d/2$, the Hamiltonian (2) can be developed into two subspaces. Each subspace has a symmetric spectrum in the up-and-down direction, so they both have chiral symmetry. Notice that when $d \neq 0$, the model becomes similar to the Rice-Mele model [52]. Then we compute the Zak phase by using the analytical formalism and the numerical methods in Eqs. (3) and (4), respectively. They have been used extensively in previous work on the calculations of the topological phases in one dimension [28,34,53–57].

$$\gamma_n = i \int_{-\pi}^{\pi} dk \langle u_n(k)|\partial_k|u_n(k)\rangle. \qquad (3)$$

Here $u_n(k)$ is the Bloch wave function. We can still use Eq. (3) to compute the Zak phase analytically if there are fewer than four nonzero hopping parameters. However, for models with four nonzero parameters, we need to use the following numerical formalism:

$$\gamma_n = \mathrm{Mod}\left(i \ln\left[\prod_{s=1}^{M} \langle u_n(k_s)|u_n(k_{s+1})\rangle\right], 2\pi\right). \qquad (4)$$

Here $u_n(k_s)$ is the eigenvector of the Hamiltonian at k_s, n labels the band, and k_s runs from $-\pi$ to π. We tested the numerical robustness of our computational methods by using a series of different numbers of discretized points up to 1×10^6. We found that 1×10^5 points are sufficient for the accuracy.

We carried out calculations for finite chains with an even (100) and odd (101) number of sites to illustrate the nature of the topological edge states related to the periodic-structure results presented in the previous sections. For the even chain, we cut off CT3 and CT4 in the rightmost cell, whereas for the odd chain, we cut off the LE2 and CT1–CT4. The amplitudes for the individual sites in the eigenvectors are computed using the populations on the LE state on that site and half of those on the CT states linked to the LE state, i.e., $P_i = P_i^{\mathrm{LE}} + \frac{1}{2}(\sum_j P_j^{\mathrm{CT}})$, where i labels the site, j labels the states linked to the ith LE state, and P^{LE} and P^{CT} are the square coefficients of the LE and CT states, respectively.

When producing the absorption spectra, we followed the methods detailed in Ref. [48]. We assumed the oscillator strengths for LE and CT are 1 and 0.1, respectively. We used a Gaussian-type broadening of $0.1t_1$. As the model takes into account only the relative energy difference between the LE and CT states, we also included a rigid energy shift of $2t_1$ in the calculations of the absorption spectra.

III. RESULTS AND DISCUSSION

A. Topological phase induced by decoupling and the chiral superposition

When turning on only intercell coupling t_1' or t_2', we can obtain the topologically nontrivial state with a mathematical structure similar to that in the SSH model, as shown in Sec. I of the Supplemental Material (SM) [58]. When turning on two hopping parameters (at least one intercell), we can see the interference between the topological states, and the Zak phase of the flat bands is qualitatively consistent with previous work [51], as shown in Sec. I of the SM. Because the flat bands are doubly degenerate (orthogonalized through the Gram-Schmidt method [59]), the total Berry phase for the degenerate multiband case can be computed [60].

We compute all 12 combinations for the parameter set $t_1, t_2, t_1', t_2' \in \{0, 1, x, y\}$ (x and y are nonzero) and tabulate the analytical formulas for the computed Zak phases in Sec. II of the SM. In this case, all the bands are flat owing to the decoupling (one of the hopping parameters is zero). We show here a typical example for $t_1 = 0$, $t_2 = 1$, $t_1' = x$, and $t_2' = y$ in Table I. When $x = y$ ($x = -y$), the Zak phases of the third and fourth (fifth and sixth) bands are π; the opposite energies of these bands show that they contain chiral symmetry. This is also true for zero-mode flat bands. For $x = y$, the two associated eigenvectors are $v_3 = \frac{1}{2}[e^{-ik}(|\mathrm{LE1}\rangle - |\mathrm{CT1}\rangle) - (|\mathrm{LE2}\rangle - |\mathrm{CT2}\rangle)]$ and $v_4 = \frac{1}{2}[-e^{-ik}(|\mathrm{LE1}\rangle + |\mathrm{CT1}\rangle) + (|\mathrm{LE2}\rangle + |\mathrm{CT2}\rangle)]$. The groups of exciton components $\{|\mathrm{LE1}\rangle, |\mathrm{CT1}\rangle\}$ and $\{|\mathrm{LE2}\rangle, |\mathrm{CT2}\rangle\}$ can be defined as a "chiral superposition" (CS), which is named after the chiral symmetry found in those states, as shown in Fig. 2(b). The left-hand (L) CS (color-coded in orange) is therefore formed by LE1 and CT1 coupled by t_2, while the right-hand (R) CS (color-coded in blue) is formed by LE2 and CT2. These two CSs are decoupled by t_1, which is the key to resuming chiral symmetry and rendering the topologically nontrivial band. In Fig. S2 of the SM, we show more examples of the scenarios with a Zak phase of π, which have similar features.

The zero-mode flat bands have a Zak phase of π when $|x^2 - y^2| = 1$, which has symmetry with $t_1' \Leftrightarrow t_2'$. We analyze and compare the associated eigenvectors for two cases, (1) $\{1, 0, 1, 0\}$ and (2) $\{0, 1, x, y\}$, with $|x^2 - y^2| = 1$, in Figs. 2(c) and 2(d), respectively. In both scenarios, the sum of the phases for the flat bands is π. These flat bands are formed by the four CT excitons. We can also apply the concept of CS to form the L and R states. For $\{1, 0, 1, 0\}$, the LCS and RCS are decoupled by t_2 [Fig. 2(c)]. As shown in Fig. 2(d), the LCS is formed by CT2–CT4 (coupled by t_1', t_2, and t_2'), and the RCS is formed by CT1; the two are decoupled by t_1. In summary, we can see that (1) when we can clearly decouple the groups of states within a cell, we will have a phase of π, assisted by the symmetry of the hopping parameters, and (2) once the symmetry of the hopping parameters is broken, a fractional phase will appear. For the first scenario, we have $t_1 = t_1'$ and $t_2 = t_2'$. For the second scenario, we can break the symmetry of swapping: $t_1' \Leftrightarrow t_2'$. We find that the eigenvectors of the states with fractional phases have unequal distributions of population in the basis states, while those with π phases have equal distributions. About the fractional phase, we have

TABLE I. The calculated Zak phases for $t_1 = 0$, $t_2 = 1$, $t_1' = x$, and $t_2' = y$.

Eigenvalues	0 (2)	$-\sqrt{x^2 - 2xy + y^2 + 1}$	$\sqrt{x^2 - 2xy + y^2 + 1}$	$-\sqrt{x^2 + 2xy + y^2 + 1}$	$\sqrt{x^2 + 2xy + y^2 + 1}$
Zak phase	$\gamma_1 + \gamma_2$	γ_3	γ_4	γ_5	γ_6
	$\pi\left(2 - \frac{1}{(x+y)^2+1} - \frac{1}{(x-y)^2+1}\right)$	$\frac{\pi(x^2-2xy+y^2+2)}{2(x^2-2xy+y^2+1)}$	$\frac{\pi(x^2-2xy+y^2+2)}{2(x^2-2xy+y^2+1)}$	$\frac{\pi(x^2+2xy+y^2+2)}{2(x^2+2xy+y^2+1)}$	$\frac{\pi(x^2+2xy+y^2+2)}{2(x^2+2xy+y^2+1)}$

following speculations: (1) the corresponding physical quantity that can be fractionalized could be the photocurrent related to the excitons, and (2) the $\pi/2$ phase may be considered to be the consequence of the quantum interference. However, these speculations need further theoretical or experimental works to validate. In addition, compared with the partons in the fractional quantum Hall effect, the states with fractional phases are similar to the partons carrying fractional charge because the linear combination of these states can offer an integer phase.

B. Topologically nontrivial zero-mode flat bands for uniform chains

For uniform chains, we have $t_1 = t_1' = 1$ and $t_2 = t_2' = x$. The Zak phases for the bottom two bands are π when $x \simeq \pm(\sqrt{2} - 1)$, as shown in Fig. 3(a). It is unexpected that we can have a topologically nontrivial band even for a uniform chain in this model. For $x \simeq \sqrt{2} - 1$, we analyze the eigenvectors at the Γ point, for which the coefficients for the individual exciton states in the eigenvector with a Zak phase of π are shown in Fig. 3(c). The CSs can be formed by the states in orange (L) and in blue (R); their coefficients have opposite signs with the same magnitude. In this case, we have chiral-symmetry swapping, LE1 ⇔ LE2, CT1 ⇔ CT3, and CT2 ⇔ CT4, which is a translational operation and symmetric for the Hamiltonian of a uniform chain. In addition, when t_2 and t_2' approach zero (but are still nonzero), the sum of the phases for the bottom two degenerate bands is $\frac{5}{2}\pi$ (equivalently, $\frac{1}{2}\pi$), which is different from the model with $t_1 = t_1' = 1$ and $t_2 = t_2' = 0$ ($\frac{3}{2}\pi$), indicating a phase transition due to the decoupling ($t_2 = t_2' = 0$). As illustrated in Figs. 3(b) and 3(c), the coupling

map changes from stripes ($t_2 = t_2' = 0$) to cross nets (all the couplings are turned on). Most importantly, we find the Zak phase of the zero-mode (or the middle two bands for nonzero d) flat bands is *always* equal to π for the uniform chain with any energy gap d according to our calculations with $d \neq 0$, whose Hamiltonian is shown in Sec. VI of the SM. The eigenvector of the flat band for the uniform chain with any d reads $v_k = A^{-\frac{1}{2}}[0, -e^{ik}t_1 - t_2, t_1 + e^{-ik}t_2]$, where $A = 2[t_1^2 + t_2^2 + 2t_1t_2 \cos(k)]$. Then the Zak phase of this state can be computed analytically as $z = i \int_{-\pi}^{\pi} v_k^* \partial_k v_k dk = -\pi$. This can also be interpreted as the inversion-symmetry-protected topological phase. Moreover, when $x \to \infty$, the phases for the bottom two bands with negative energies will approach $\frac{1}{4}\pi$ asymptotically, leading to a phase sum of $\frac{1}{2}\pi$, which is consistent with the uniform-chain calculation shown in the Sec. VI of the SM. This is different from the case for $t_1 = t_1' = 0$ and $t_2 = t_2' = 1$ (the Zak phase is $\frac{3}{2}\pi$) due to the symmetry and quantum interference.

C. The Dexter-type topological phase transition

We have studied the scenario where $t_1 = t_2 = 1$ and $t_1' = x$ and $t_2' = y \neq x$ for topological phase transitions. The Zak phases for the bottom two bands as a function of x and y are shown in Figs. 4(a) and 4(b). When $|t_1't_2'| = 1$, there is a phase transition, as suggested by the Zak phase between $-\frac{\pi}{2}$ and $\frac{\pi}{2}$ when tuning the hopping parameter continuously, which is more remarkable when compared with the aforementioned decoupling mechanism. This topological phase transition is due to the Dexter-type excitonic hopping effect [61] between LE1 and LE2 in which the effective hopping strengths for the entire exciton are $T = 2t_1t_2$ and $T' = 2t_1't_2'$ (T and T' are
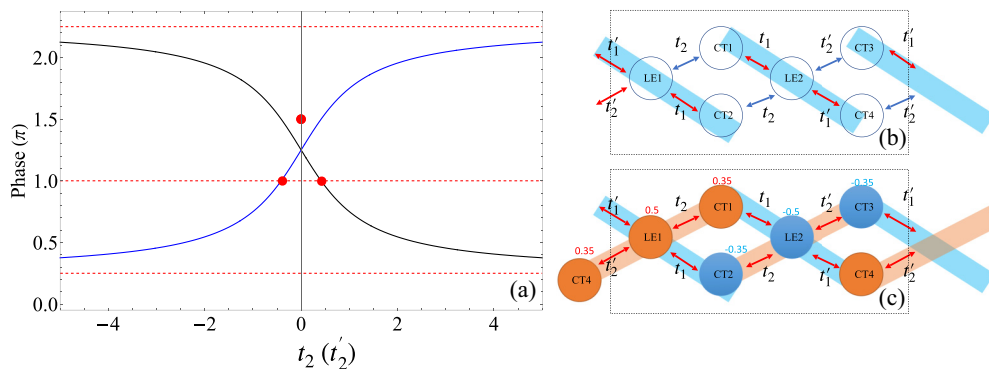

FIG. 3. (a) The Zak phases for the bottom two bands (the lowest band in blue) as a function of $t_2 = t_2' = x$ for a uniform chain ($t_1 = t_1' = 1$). The phases down to $t_2 = -0.01$ ($t_2 = 0.01$) from the left-hand side (right-hand side) are plotted. Notice that the phase could be π even for a uniform chain at $t_2 = t_2' \simeq \pm(\sqrt{2} - 1)$. The red points indicate the phase of $\frac{3}{2}\pi$ for the case with $t_1 = t_1' = 1$ and $t_2 = t_2' = 0$. Therefore, there is a phase transition at $x = 0$, changing from $\frac{1}{2}\pi$ to $\frac{3}{2}\pi$. On the other hand, when x goes to infinity, the phases will approach $\frac{1}{4}\pi$ asymptotically. The coupling maps are shown when $t_2 = t_2' = 0$ in (b) and $t_2 = t_2' \neq 0$ in (c), with $t_1 = t_1' = 1$. The coefficients are shown for the eigenvector with a Zak phase of π for $t_1 = t_1' = 1$ and $t_2 = t_2' \simeq \pm(\sqrt{2} - 1)$. The coefficients have opposite signs for the member states in the LCS and RCS, as shown in (c).
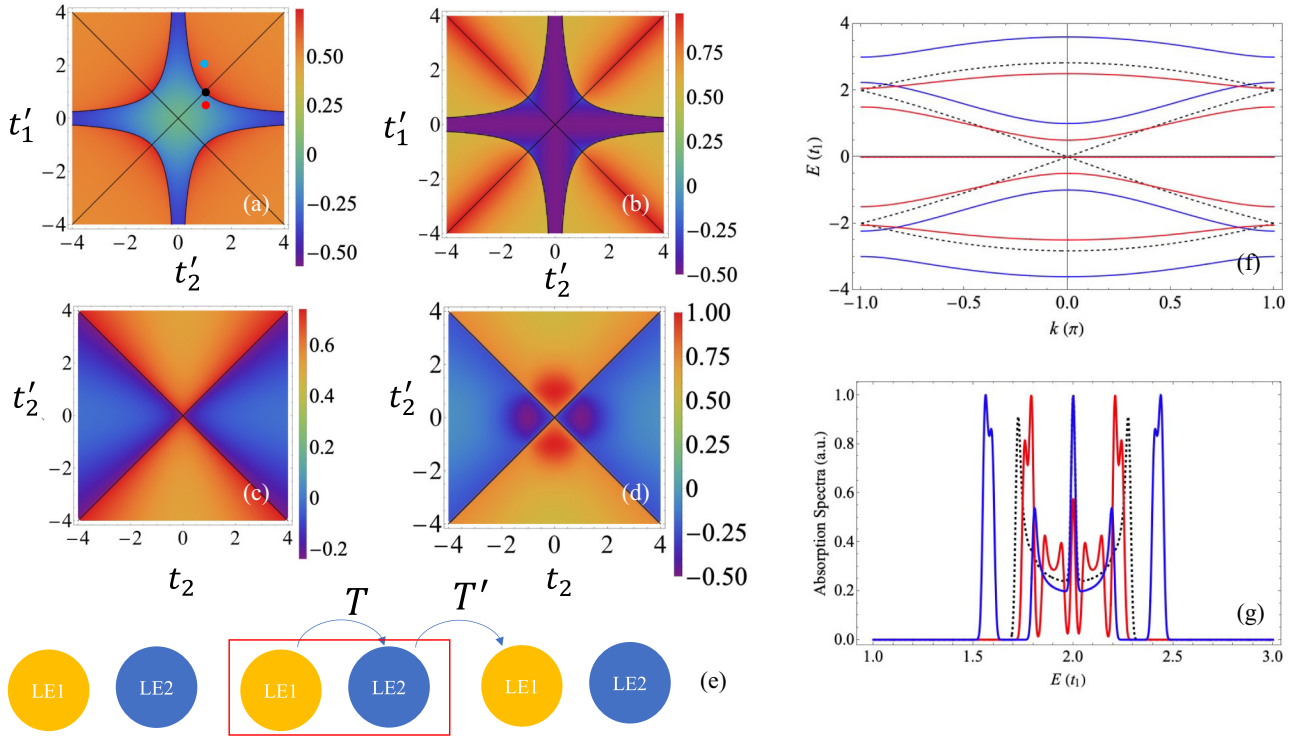
FIG. 4. The Zak phases (in units of π) for the bottom two bands computed for (a) and (b) $t_1 = t_2 = 1$ as a function of t_1' and t_2' and (c) and (d) $t_1 = t_1' = 1$ as a function of t_2 and t_2'. (e) The phase transition mechanism. (f) The color-coded band structures and (g) corresponding absorption spectra for the parameters at the blue ($t_1' = 1, t_2' = 2$), black dashed ($t_1' = 1, t_2' = 1$), and red ($t_1' = 1, t_2' = \frac{1}{2}$) points indicated in (a).

illustrated in Fig. 1). Here the condition for the phase transition is that $|T| = |T'|$, which is similar to the situation when the cross-cell hopping is equal to the intracell hopping in the SSH model, as shown in Fig. 4(e). This phase transition is also consistent with previous work on the measurement of phase difference [62]. However, the carriers for the phase transition change to excitons, which is entirely different from the conventional SSH and Rice-Mele models. This phase transition is further supported by our calculations for $t_1 = t_1' = 1$ and $t_2 = x$ and $t_2' = y$ [Figs. 4(c) and 4(d)], showing a linear relationship between t_2 and t_2' at the phase transition. In Figs. 4(f) and 4(g), the band structures and corresponding normalized optical absorption spectra at the red ($t_1 = t_2 = 1, t_1' = 1, t_2' = \frac{1}{2}$), black ($t_1 = t_2 = 1, t_1' = 1, t_2' = 1$), and blue ($t_1 = t_2 = 1, t_1' = 1, t_2' = 2$) points in Fig. 4(a) are shown to demonstrate the phase transition. From the band structures, we can see the band gap closing at $k = 0$ and $k = \pm\pi$, which implies that these two phases are disconnected adiabatically.

Further calculations show that this type of phase transition can survive from the nonzero energy gap d, suggesting its robustness against perturbations and further broadening the applicability of our model. This type of phase transition was reported previously [62] within the Rice-Mele model realized in the optical lattice. In relation to that, LE1 and LE2 are coupled by the CT states, which will open a gap between them, corresponding to the on-site energy offset between the neighboring sites in the Rice-Mele model. Notice that we also have another transition when $|t_1'| = |t_2'|$ owing to a change in the symmetry, which is fundamentally different. We show the results for this situation in Fig. S3 in the SM. The products of

the hopping integrals were also recently explored to identify the number of edge states in a four-band SSH model [63].

Moreover, as the zero-mode flat bands are of great interest, we also studied the phase sum for the scenario of $\{x, y, 1, 1\}$, where, generally, $x \neq y$. Then the phase sum is equal to $\pi|x^2 - y^2|$, which is π when $|x^2 - y^2| = 1$. We also derived the Zak phase formalism for the general scenario $\{1, x, y, z\}$, as shown in Sec. IV of the SM, where, in general, x, y, and z are nonzero and unequal to each other. Here we need to point out that the twofold degeneracy of the flat bands is robust against any perturbation including nonzero d, which implies the existence of the topological edge states [64].

D. The edge states in the finite chains

The finite chain calculations with 100 sites were performed for the even chain using the four parameter sets discussed in the previous sections, i.e., $\{1, 0, t_1' = x, 0\}$, $\{1, t_2, 1, t_2' = t_2\}$, $\{0, 1, t_1', \sqrt{1 + t_1'^2}\}$, and $\{1, 1, t_1', t_1' + 1\}$, as shown in Fig. 5. Here we compute the eigenvalues as a function of t_1' or t_2 in Figs. 5(a), 5(d), 5(g), and 5(j) and the site-dependent amplitude distributions for (1) the edge states in the zero-mode flat bands in Figs. 5(b), 5(e) 5(h), and 5(k) and (2) the additional interesting quasiedge states in Figs. 5(c), 5(f), 5(i), and 5(l). Because there are more than two states with zero energy, we call the edge states "zero-mode edge states" here to distinguish them. As shown in the second row of Fig. 5, each zero-mode edge state is localized on only one end of the chain, and two zero-mode edge states will not appear on the same side (one end has only one state, which is consistent with the symmetric nature of the even chain model). By
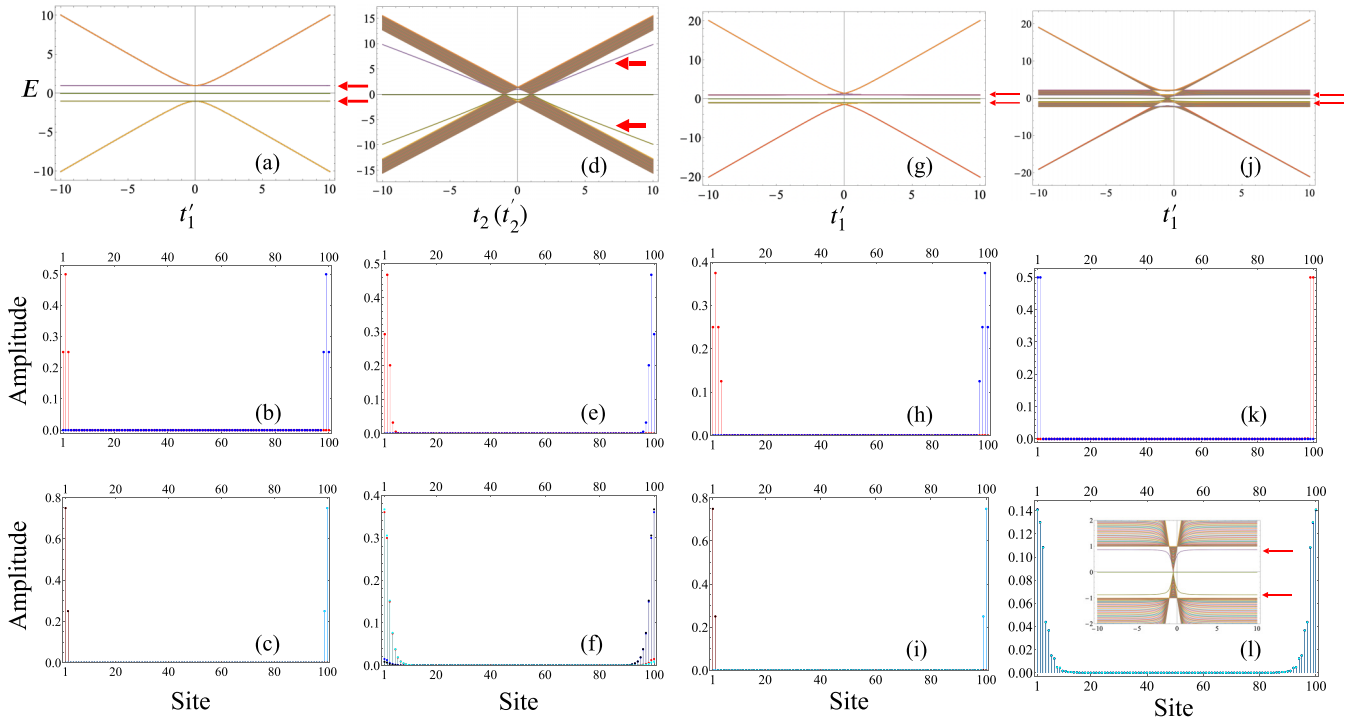
FIG. 5. (a), (d), (g), and (j) The eigenvalues and (b), (c), (e), (f), (h), (i), (k), and (l) the cell amplitudes of a finite chain with 100 sites for different parameter sets. The second row of plots shows the amplitudes of the eigenvectors for the edge states of the zero-mode flat bands. The red arrows point to the edge states chosen for the plots of amplitudes in the third row. The parameter sets are $\{1, 0, t_1', 0\}$ for (a), $\{1, 0, 1, 0\}$ for (b) and (c), $\{1, t_2, 1, t_2' = t_2\}$ for (d), $\{1, \sqrt{2} - 1, 1, \sqrt{2} - 1\}$ for (e) and (f), $\{0, 1, t_1', \sqrt{1 + t_1'^2}\}$ for (g), $\{0, 1, 1, \sqrt{2}\}$ for (h) and (i), $\{1, 1, t_1', t_1' + 1\}$ for (j), and $\{1, 1, 2, 3\}$ for (k) and (l). Note that the zoom-in spectra are plotted for (l) to illustrate the edge state which is far off from the bulk states. We can see the edge modes for these scenarios for the zero-mode flat bands, especially for the uniform chain in (d)–(f).

comparing these results with the infinite chain results, it can be seen that each zero mode in the infinite chain corresponds to one zero-mode edge state in the even chain. This correspondence will help us in the odd chain calculations later. Recalling the Zak phase results for the relevant edge states in the infinite chain calculations, it can be seen that these edge states are topologically nontrivial and protected by the inversion symmetry. In particular, the edge state in the zero-mode flat bands further confirms the topologically nontrivial bands for the uniform chain [Fig. 5(e)]. We also find that the edge mode for a uniform chain will be more localized as we increase the strength of t_2 (or t_2'). Apart from the zero-mode edge states, we use red arrows to label the eigenvalues for these quasiedge states in Fig. 5. As shown in Figs. 5(a), 5(g), and 5(j), the edge states are the flat bands pointed to by the red arrows for the cases $\{1, 0, t_1', 0\}$ and $\{0, 1, t_1', \sqrt{1 + t_1'^2}\}$, whereas the edge states appear off from the bulk states for $\{1, t_2, 1, t_2\}$ (the uniform chain). For the case with $\{0, 1, 2, 2\}$, we find the bands with an energy of 1 are topological, which is consistent with the corresponding infinite chain calculations (see Table I). The amplitude distributions of the edge states in the four parameter sets, computed for $\{1, 0, 1, 0\}$, $\{1, \sqrt{2} - 1, 1, \sqrt{2} - 1\}$, $\{0, 1, 1, \sqrt{2}\}$, and $\{1, 1, 2, 3\}$, show a consistent trend. For the $\{1, 0, 1, 0\}$ case, the edge states are concentrated on both of the edge sites, with four associated quasiedge states (bonding/antibonding on each end). For the

other three cases, the amplitudes decay exponentially from the edge towards the center of the chain.

For an odd number of sites, we find that the edge state can be asymmetric (as it concentrates on only one end) for nonuniform chains, which is apparently due to the asymmetric structure of the odd-number chain. Here we define that the odd chain labeled by the parameters $\{t_1, t_2, t_1', t_2'\}$ has a left end starting with t_1 and t_2 and a right end starting with t_1' and t_2'. It is convenient to compare the state localized at the right end of an odd chain with $\{t_1, t_2, t_1', t_2'\}$ with the state localized at the right end of an even chain with $\{t_1', t_2', t_1, t_2\}$. Here we take an interesting case in which the even chain cases with $\{1, \sqrt{2}, 0, 1\}$ and $\{0, 1, 1, \sqrt{2}\}$ both have topological nontrivial zero modes as an example. It can be seen that there are two different edge states localized at the two ends of the odd chain for $\{1, \sqrt{2}, 0, 1\}$ in Fig. 6(b). By comparing the odd chain result in Fig. 6(b) with relevant even chain cases [Figs. 5(h) and 6(a)], it can be seen that each zero-mode edge state in the odd chain case shares the exact same eigenvector with one of the zero-mode edge states in the relevant even chain case. Considering that each zero-mode edge state in the even chain cases is localized at only one end and corresponds to one of the zero-mode flat bands in the infinite chain calculations, we can take two states from each of the corresponding infinite chain calculations to calculate the Zak phase in the odd chain cases. The results show that the sum of the Zak phases of the
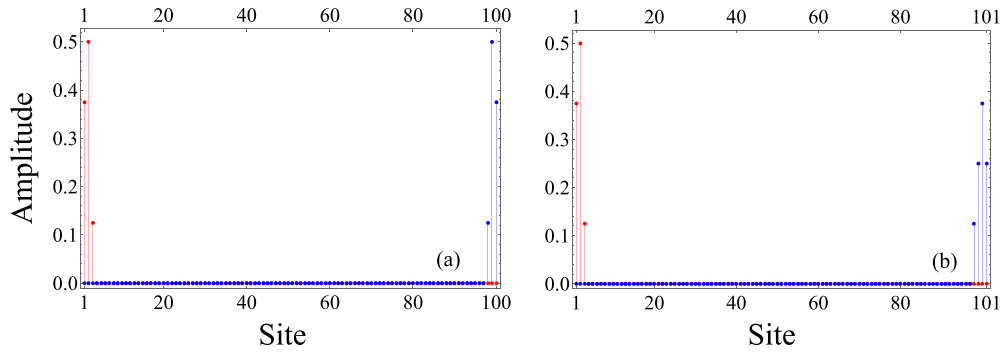
FIG. 6. The amplitudes of the sites for finite chains with an (a) even and (b) odd number of sites: (a) 100 sites for $\{1, \sqrt{2}, 0, 1\}$ and (b) 101 sites for $\{1, \sqrt{2}, 0, 1\}$. Notice that the amplitudes become asymmetric for the odd chains.

chosen states is always zero for the finite chain. This means that, although the eigenvectors of the edge states are the same, the edge states are trivial states for the odd chain cases because the inversion symmetry is broken.

E. Experimental design for the observation of excitonic edge states

Our model strongly indicates that there could be either edge states in the zero-mode flat bands or quasiedge states in the bands split off from the main bands. It could therefore be straightforward to observe the topological edge states in the following experimental setup. The most convenient experimental materials platform could be the molecular chains in nanowires [28,65]. In particular, the highest occupied molecular orbitals (HOMOs) and the lowest unoccupied molecular orbitals (LUMOs) are well separated in porphyrinlike molecular chains, such as copper phthalocyanine (CuPc) [65–69]. Although the LUMO states are doubly degenerate (e_{gx} and e_{gy} under D_{4h} symmetry), they can be decoupled approximately by symmetry. In addition, the HOMO (a_{1u} state) is almost decoupled from the rest of the orbitals. Moreover, the interchain coupling can be neglected as shown in previous work [48]. To observe the topological edge states, we first synthesize the CuPc molecular nanowires, which are then diluted such that we can separate individual nanowires. After this, the diluted nanowire sample can be deposited on the quartz or Perylenetetracarboxylic dianhydride through annealing [28]. We then shed the laser at the wavelengths near the two peaks of the Q bands [65,66] because the middle of the two peaks for the Q band corresponds to the zero mode and the two peaks correspond to the band edges in the exciton band structure, supposing the LE and CT states are almost degenerate. The hopping integrals are on the order of 0.1 eV, following [48]. To observe the edge states in Fig. 5(f), we need to focus the light wavelength to $\sim \pm t$ near the zero mode [as shown by the split-off energy levels in Figs. 5(d), 5(g), and 5(j)], which is between 635 and 710 nm if the zero mode corresponds to 670 nm (the pink region in Fig. 7). Through photoluminescence spectroscopy we expect to observe the light emission concentrated on both ends of the chain, as shown in Fig. 7. To observe the topological phase transition assisted by the Dexter process, we need to be able to tune the interaction, which can be realized in the optical lattice [70,71]. Alternatively, the dimerization between molecules can be realized through ligand engineering.

IV. CONCLUSIONS

In summary, we studied the excitonic topological properties of a one-dimensional model that takes into account the dimerization and the LE and CT excited states. We found (1) a topological phase transition assisted by the Dexter electron exchange for the excitonic hopping and (2) the topologically nontrivial phase of π for the zero-mode flat bands can exist even for a uniform chain with any energy gap d, especially the robustness of the degeneracy for the zero-mode flat bands. In addition, we developed the concept of chiral superposition to understand the topological phase. Our finite chain calculations further confirmed our periodic-structure calculations: the zero-mode edge states in the even chain cases are topologically nontrivial, which is protected by the inversion symmetry; these states will become trivial states in the odd chain cases as the inversion symmetry is broken. Based on the studies of the topological edge states in one dimension, we designed an experiment to observe them optically in the molecular chains in the UV-visible spectral region.

All the computer codes and data that support the findings of this study are available from the corresponding author upon reasonable request.
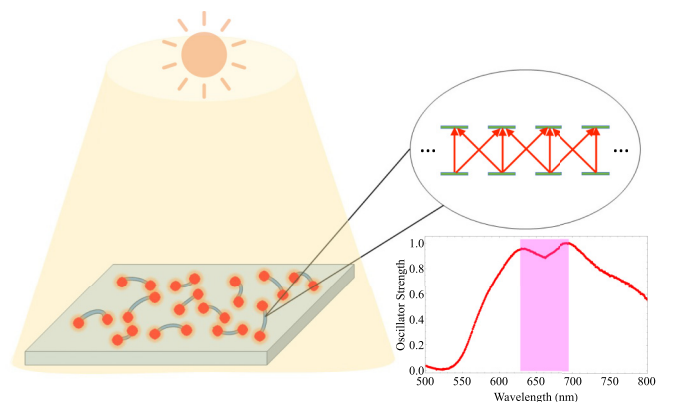

FIG. 7. The proposed experiment to observe the edge states using molecular nanowires. The diluted nanowires are deposited on the surface. By shedding the CW laser, we could observe the photoluminescence from both chain ends. One of the potential candidates is a CuPc nanowire, in which there are well-defined two-level systems, as illustrated in the zoom. The wavelength of the laser used should be situated between the two peaks of the so-called Q band of the CuPc nanowire, as illustrated in the pink area in the UV-Vis spectra.

ACKNOWLEDGMENTS

[1] C. Kittel, *Introduction to Solid State Physics* (Wiley, Hoboken, NJ, 2018).

[2] H. Deng, H. Haug, and Y. Yamamoto, Exciton-polariton Bose-Einstein condensation, Rev. Mod. Phys. **82**, 1489 (2010).

[3] S. B. Anantharaman, K. Jo, and D. Jariwala, Exciton–photonics: From fundamental science to applications, ACS Nano **15**, 12628 (2021).

[4] M. S. Dresselhaus, G. Dresselhaus, R. Saito, and A. Jorio, Exciton photophysics of carbon nanotubes, Annu. Rev. Phys. Chem. **58**, 719 (2007).

[5] S. M. Menke and R. J. Holmes, Exciton diffusion in organic photovoltaic cells, Energy Environ. Sci. **7**, 499 (2014).

[6] O. V. Mikhnenko, P. W. Blom, and T.-Q. Nguyen, Exciton diffusion in organic semiconductors, Energy Environ. Sci. **8**, 1867 (2015).

[7] J. Lee, P. Jadhav, P. D. Reusswig, S. R. Yost, N. J. Thompson, D. N. Congreve, E. Hontz, T. Van Voorhis, and M. A. Baldo, Singlet exciton fission photovoltaics, Acc. Chem. Res. **46**, 1300 (2013).

[8] Y. Xu, P. Xu, D. Hu, and Y. Ma, Recent progress in hot exciton materials for organic light-emitting diodes, Chem. Soc. Rev. **50**, 1030 (2021).

[9] B. Zhang and L. Sun, Artificial photosynthesis: Opportunities and challenges of molecular catalysts, Chem. Soc. Rev. **48**, 2216 (2019).

[10] A. Stirbet, D. Lazár, Y. Guo, and G. Govindjee, Photosynthesis: Basics, history and modelling, Ann. Bot. **126**, 511 (2020).

[11] M. Sarovar, A. Ishizaki, G. R. Fleming, and K. B. Whaley, Quantum entanglement in photosynthetic light-harvesting complexes, Nat. Phys. **6**, 462 (2010).

[12] J. B. Derr, J. Tamayo, J. A. Clark, M. Morales, M. F. Mayther, E. M. Espinoza, K. Rybicka-Jasińska, and V. I. Vullev, Multifaceted aspects of charge transfer, Phys. Chem. Chem. Phys. **22**, 21583 (2020).

[13] L.-S. Cui *et al.*, Fast spin-flip enables efficient and stable organic electroluminescence from charge-transfer states, Nat. Photon. **14**, 636 (2020).

[14] G. Han and Y. Yi, Local excitation/charge-transfer hybridization simultaneously promotes charge generation and reduces nonradiative voltage loss in nonfullerene organic solar cells, J. Phys. Chem. Lett. **10**, 2911 (2019).

[15] V. W.-W. Yam, A. K.-W. Chan, and E. Y.-H. Hong, Charge-transfer processes in metal complexes enable luminescence and memory functions, Nat. Rev. Chem. **4**, 528 (2020).

[16] J. Guillet, *Polymer Photophysics and Photochemistry* (Cambridge University Press, New York, 1985).

[17] T. Ozawa *et al.*, Topological photonics, Rev. Mod. Phys. **91**, 015006 (2019).

[18] L. Lu, J. D. Joannopoulos, and M. Soljačić, Topological photonics, Nat. Photon. **8**, 821 (2014).

[19] Y. Ota, K. Takata, T. Ozawa, A. Amo, Z. Jia, B. Kante, M. Notomi, Y. Arakawa, and S. Iwamoto, Active topological photonics, Nanophotonics **9**, 547 (2020).

[20] M. Kim, Z. Jacob, and J. Rho, Recent advances in 2D, 3D and higher-order topological photonics, Light: Sci. Appl. **9**, 130 (2020).

[21] M. Segev and M. A. Bandres, Topological photonics: Where do we go from here? Nanophotonics **10**, 425 (2020).

[22] Y. Wu, C. Li, X. Hu, Y. Ao, Y. Zhao, and Q. Gong, Applications of topological photonics in integrated photonic devices, Adv. Opt. Mater. **5**, 1700357 (2017).

[23] H. Price *et al.*, Roadmap on topological photonics, J. Phys. Photon. **4**, 032501 (2022).

[24] J. N. Crain and D. T. Pierce, End states in one-dimensional atom chains, Science **307**, 703 (2005).

[25] C. F. Hirjibehedin, C. P. Lutz, and A. J. Heinrich, Spin coupling in engineered atomic structures, Science **312**, 1021 (2006).

[26] A. A. Khajetoorians, D. Wegner, A. F. Otte, and I. Swart, Creating designer quantum states of matter atom-by-atom, Nat. Rev. Phys. **1**, 703 (2019).

[27] D.-J. Choi, N. Lorente, J. Wiebe, K. von Bergmann, A. F. Otte, and A. J. Heinrich, Colloquium: Atomic spin chains on surfaces, Rev. Mod. Phys. **91**, 041001 (2019).

[28] Y. Zhao *et al.*, Quantum nanomagnets in on-surface metal-free porphyrin chains, Nat. Chem. **15**, 53 (2023).

[29] A. R. Murad, A. Iraqi, S. B. Aziz, S. N. Abdullah, and M. A. Brza, Conducting polymers for optoelectronic devices and organic solar cells: A review, Polymers **12**, 2627 (2020).

[30] J. M. Nichol, Quantum-dot spin chains, in *Entanglement in Spin Chains: From Theory to Quantum Technology Applications*, edited by A. Bayat, S. Bose, and H. Johannesson (Springer, Cham, 2022), pp. 505–538.

[31] M. Kiczynski, S. Gorman, H. Geng, M. Donnelly, Y. Chung, Y. He, J. Keizer, and M. Simmons, Engineering topological states in atom-based semiconductor quantum dots, Nature (London) **606**, 694 (2022).

[32] W. P. Su, J. R. Schrieffer, and A. J. Heeger, Solitons in polyacetylene, Phys. Rev. Lett. **42**, 1698 (1979).

[33] W. P. Su, J. R. Schrieffer, and A. J. Heeger, Soliton excitations in polyacetylene, Phys. Rev. B **22**, 2099 (1980).

[34] J. Zak, Berry's phase for energy bands in solids, Phys. Rev. Lett. **62**, 2747 (1989).

[35] J. K. Asbóth, L. Oroszlány, A. Pályi, J. K. Asbóth, L. Oroszlány, and A. Pályi, *A Short Course on Topological Insulators: Band Structure and Edge States in One and Two Dimensions* (Springer International Publishing, Switzerland, 2016).

[36] D. Leykam and S. Flach, Perspective: Photonic flatbands, APL Photon. **3**, 070901 (2018).

[37] E. J. Bergholtz and Z. Liu, Topological flat band models and fractional Chern insulators, Int. J. Mod. Phys. B **27**, 1330017 (2013).

[38] L. Balents, C. R. Dean, D. K. Efetov, and A. F. Young, Superconductivity and strong correlations in moiré flat bands, Nat. Phys. **16**, 725 (2020).

[39] R. A. Vicencio Poblete, Photonic flat band dynamics, Adv. Phys. X **6**, 1878057 (2021).

[40] O. Derzhko, J. Richter, and M. Maksymenko, Strongly correlated flat-band systems: The route from Heisenberg spins to Hubbard electrons, Int. J. Mod. Phys. B **29**, 1530007 (2015).

[41] Z. Liu, F. Liu, and Y.-S. Wu, Exotic electronic states in the world of flat bands: From theory to material, Chin. Phys. B **23**, 077308 (2014).

[42] L. Tang, D. Song, S. Xia, S. Xia, J. Ma, W. Yan, Y. Hu, J. Xu, D. Leykam, and Z. Chen, Photonic flat-band lattices and unconventional light localization, Nanophotonics **9**, 1161 (2020).

[43] F. Wu, T. Lovorn, and A. H. MacDonald, Topological exciton bands in moiré heterojunctions, Phys. Rev. Lett. **118**, 147401 (2017).

[44] T. Gao, O. A. Egorov, E. Estrecho, K. Winkler, M. Kamp, C. Schneider, S. Höfling, A. G. Truscott, and E. A. Ostrovskaya, Controlled ordering of topological charges in an exciton-polariton chain, Phys. Rev. Lett. **121**, 225302 (2018).

[45] D. Varsano, M. Palummo, E. Molinari, and M. Rontani, A monolayer transition-metal dichalcogenide as a topological excitonic insulator, Nat. Nanotechnol. **15**, 367 (2020).

[46] R. Wang, T. A. Sedrakyan, B. Wang, L. Du, and R.-R. Du, Excitonic topological order in imbalanced electron–hole bilayers, Nature (London) **619**, 57 (2023).

[47] R. Mori, S. Ciocys, K. Takasan, P. Ai, K. Currier, T. Morimoto, J. E. Moore, and A. Lanzara, Spin-polarized spatially indirect excitons in a topological insulator, Nature (London) **614**, 249 (2023).

[48] Q. Chen, J. Chang, L. Ma, C. Li, L. Duan, X. Ji, J. Zhang, W. Wu, and H. Wang, Optoelectronic properties of one-dimensional molecular chains simulated by a tight-binding model, AIP Adv. **11**, 015127 (2021).

[49] A. Armin et al., A history and perspective of non-fullerene electron acceptors for organic solar cells, Adv. Energy Mater. **11**, 2003570 (2021).

[50] Y. Wang, J. Lee, X. Hou, C. Labanti, J. Yan, E. Mazzolini, A. Parhar, J. Nelson, J.-S. Kim, and Z. Li, Recent progress and challenges toward highly stable nonfullerene acceptor-based organic solar cells, Adv. Energy Mater. **11**, 2003002 (2021).

[51] G. H. Reid, M. Lu, A. R. Fritsch, A. M. Piñeiro, and I. B. Spielman, Dynamically induced symmetry breaking and out-of-equilibrium topology in a 1d quantum system, Phys. Rev. Lett. **129**, 123202 (2022).

[52] M. J. Rice and E. J. Mele, Elementary excitations of a linearly conjugated diatomic polymer, Phys. Rev. Lett. **49**, 1455 (1982).

[53] P. Delplace, D. Ullmo, and G. Montambaux, Zak phase and the existence of edge states in graphene, Phys. Rev. B **84**, 195452 (2011).

[54] R. Resta, Manifestations of Berry's phase in molecules and condensed matter, J. Phys.: Condens. Matter **12**, R107 (2000).

[55] N. H. Le, A. J. Fisher, N. J. Curson, and E. Ginossar, Topological phases of a dimerized Fermi–Hubbard model for semiconductor nano-lattices, npj Quantum Inf. **6**, 24 (2020).

[56] J. Zhu, W. Wu, and A. J. Fisher, Linear combination of atomic orbitals model for deterministically placed acceptor arrays in silicon, Phys. Rev. B **101**, 085303 (2020).

[57] J. Zhu, W. Wu, and A. J. Fisher, Multihole models for deterministically placed acceptor arrays in silicon, Phys. Rev. B **104**, 125415 (2021).

[58] See Supplemental Material at http://link.aps.org/supplemental/10.1103/PhysRevB.110.085418 for (1) the results of the calculations with one or two non-zero parameters, (2) the Zak phases of all possible cases with three non-zero parameters, (3) more examples for the chiral superposition, (4) the Zak phases of the zero-mode flat bands for {1,x,y,z} case, and (5) the details of the diagonal lines in Fig. 4(a).

[59] W. Cheney and D. Kincaid, Linear Algebra: Theory and Applications, The Jones & Bartlett Learning International Series in Mathematics (Jones & Bartlett Learning, USA, 2012).

[60] D. Vanderbilt, Berry Phases in Electronic Structure Theory: Electric Polarization, Orbital Magnetization and Topological Insulators (Cambridge University Press, Cambridge, 2018).

[61] W. Wu, A. Kerridge, A. H. Harker, and A. J. Fisher, Structure-dependent exchange in the organic magnets Cu(II)Pc and Mn(II)Pc, Phys. Rev. B **77**, 184403 (2008).

[62] M. Atala, M. Aidelsburger, J. T. Barreiro, D. Abanin, T. Kitagawa, E. Demler, and I. Bloch, Direct measurement of the Zak phase in topological Bloch bands, Nat. Phys. **9**, 795 (2013).

[63] C.-S. Lee, I.-F. Io, and H.-C. Kao, Winding number and Zak phase in multi-band SSH models, Chin. J. Phys. **78**, 96 (2022).

[64] X.-G. Wen, A theory of 2+1D bosonic topological orders, Natl. Sci. Rev. **3**, 68 (2016).

[65] H. Wang et al., Ultralong copper phthalocyanine nanowires with new crystal structure and broad optical absorption, ACS Nano **4**, 3921 (2010).

[66] T. Guo, T. Zou, P. Shi, Y. Song, M. Wu, F. Xiao, J. Zhang, W. Wu, and H. Wang, A new polymorph of zinc-phthalocyanine and its optical properties, J. Cryst. Growth **546**, 125760 (2020).

[67] M.-S. Liao and S. Scheiner, Electronic structure and bonding in metal phthalocyanines, metal= Fe, Co, Ni, Cu, Zn, Mg, J. Phys. Chem. Lett. **114**, 9780 (2001).

[68] N. Marom, X. Ren, J. E. Moussa, J. R. Chelikowsky, and L. Kronik, Electronic structure of copper phthalocyanine from G_0W_0 calculations, Phys. Rev. B **84**, 195143 (2011).

[69] W. Wu, A. J. Fisher, and N. M. Harrison, Theoretical modeling of the electronic structure and exchange interactions in a Cu(II)Pc one-dimensional chain, Phys. Rev. B **84**, 024427 (2011).

[70] E. Anisimovas, M. Raciunas, C. Sträter, A. Eckardt, I. B. Spielman, and G. Juzeliunas, Semisynthetic zigzag optical lattice for ultracold bosons, Phys. Rev. A **94**, 063632 (2016).

[71] L. J. Maczewsky, K. Wang, A. A. Dovgiy, A. E. Miroshnichenko, A. Moroz, M. Ehrhardt, M. Heinrich, D. N. Christodoulides, A. Szameit, and A. A. Sukhorukov, Synthesizing multi-dimensional excitation dynamics and localization transition in one-dimensional lattices, Nat. Photon. **14**, 76 (2020).